Alkaline earth and uranyl cation complexes of a calix[4]arene-tetraamide: MD and FEP simulations in aqueous and acetonitrile solutions and X-ray structure of its Sr(Picrate)$_2$ complex

Nicolas Muzet,[a] Georges Wipff,*[,a] Alessandro Casnati,[b] Laura Domiano,[b] Rocco Ungaro[b] and Franco Ugozzoli*[,c]

[a] *Laboratoire MSM, URA 422 CNRS, Institut de Chimie, 4, rue B. Pascal, 67 000 Strasbourg, France*

[b] *Dipartimento di Chimica Organica e Industriale, Chimica Analitica, Chimica Fisica, Universita di Parma e Centro di Studio per la Strutturistica Diffrattometrica del CNR, via delle Scienze 78, I-43100 Parma, Italy*

[c] *Dipartimento di Chimica Generale ed Inorganica, Chimica Analitica, Chimica fisica, Universita di Parma e Centro di Studio per la Strutturistica Diffrattometrica del CNR, via delle Scienze 78, I-43100 Parma, Italy*

We report the X-ray structure of the L·Sr(Picrate)$_2$ (L = *tert*-butyl-calix[4]arene-tetrakis(diethylamide)† and MD simulations on the L·M^{2+} complexes *in vacuo*, in water and in acetonitrile solutions (M^{2+} = Mg^{2+}, Ca^{2+}, Sr^{2+}, Ba^{2+}), with a comparison of 'converging' L$_C$ and 'diverging' L$_D$ conformers. In the simulated and solid-state structures of the L·Sr^{2+} complex, the cation is completely encapsulated within the polar pseudo-cavity of L, without coordination to its counterion in the crystal, or to solvent molecules in solution. Computations show that the L·M^{2+} complexes are of converging type in water and in acetonitrile. This contrasts with the L·M^{+} alkali cation complexes, which display conformational flexibility in solution. Subtle structural changes from Mg^{2+} to Ba^{2+} are compared in the gas phase and in solution. In the L·UO$_2^{2+}$ hypothetical complex, simulated for comparison, the UO$_2^{2+}$ cation is calculated to be less bound by L than the alkaline earth cations. The solvent content of the cone is shown to depend on the size of the complexed cation and modulated by the top–bottom mechanical coupling in the calixarene. Based on free energy perturbation calculations, we calculate a binding sequence of alkaline earth cations (Ca^{2+} > Sr^{2+} > Ba^{2+} > Mg^{2+}) in agreement with experiment.

Introduction

Calix[4]arene derivatives with ester, ketone and amide substituents at the lower rim display strong extracting and complexing properties toward alkali cations.[1-5] They also complex alkaline earth cations in methanol with a marked preference for Ca^{2+} and Sr^{2+} over Ba^{2+} or Mg^{2+}.[6] Their ability to discriminate between such guests can be ascribed to the preorganized cone conformation and to the binding properties of the carbonyl groups which wrap around the complexed cation. In addition to a precise knowledge of their conformational state, it is important to assess the role of solvent and of counterions on the cation binding by L. Up to now, only one related solid-state structure has been published:[7] the K$^+$ complex of *tert*-butyl-calix[4]arene-tetrakis(diethylamide) L (Fig. 1) in which the K$^+$ is encapsulated within the pseudo-cavity delineated by the four carbonyl and the four phenolic ether oxygens. The K$^+$ cation is completely shielded from the counterion, and from the solvent molecule (methanol) sitting within the cone. The relevance of this solid-state structure for the solution state of this and other alkali cation complexes can be questioned, based on molecular dynamics (MD) simulations.[8,9] Indeed, it was found that solvent may compete with the cation coordination to the putative binding sites. In protic solvents like water, we suggested that the structure of the complex results from an equilibrium between conformers where some carbonyls adopt more or less 'converging' orientations toward the cation, while others are 'diverging' to the solvent[10] (Fig. 2). In relation to these conformational states and with the solvent coordination to the complexed cation, the position of the cation was found to deviate from the K$^+$ position in the solid state and to be cation dependent. In acetonitrile solution, which displays less attraction to the carbonyl binding sites, the population of 'converging' complexes was predicted to be much higher than in water.[9]

As the charge of the cation increases, its attractions with the ligand, the solvent and its counterion also increase and it is not clear if the net balance will be in favour of 'closed' complexes with converging carbonyls or of more 'open' complexes, where the carbonyls are diverging and the cation is less shielded.

In this paper we report two complementary studies of the L·M^{2+} complexes performed independently in Parma and in Strasbourg. First, a solid-state structure of the Sr(Picrate)$_2$ complex is reported. Then, based on computer simulations, we describe the complexes of L with Mg^{2+} to Ba^{2+} alkaline earth cations in solution. The question of 'converging'/'diverging' conformation of the binding sites is compared consistently in water and in acetonitrile solutions. The uranyl complex of L$_C$ is calculated to compare the complexation of spherical/linear divalent cations in water and in acetonitrile.

A second important issue concerns the possibility to 'predict' computationally the binding selectivity of alkaline earth cations in solution. In fact, free energy perturbation (FEP) simulations on alkali cation complexes of crown ethers,[11] cryptands,[12,13] calixarenes[14-16] and naturally occurring ionophores like valinomycine[17,18] or nonactine[19] correctly reproduced the peak of binding selectivity, at least at the qualitative level. No such computations have been reported, to our knowledge, for

† IUPAC name: 1^5,3^5,5^5,7^5-tetra-*tert*-butyl-1^2,3^2,5^2,7^2-tetrakis(*N*,*N*-diethylaminocarbonylmethoxy)-1,3,5,7(1,3)-tetrabenzenacycloocta-phane.

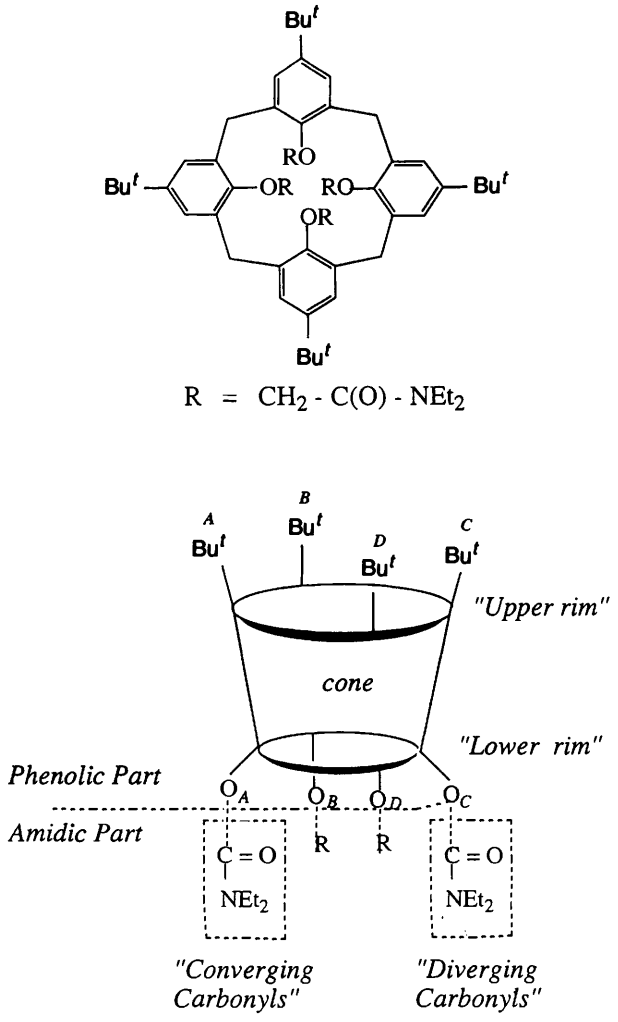

Fig. 1 The *tert*-butyl-calix[4]arene-tetradiethylamide ligand **L**

M^{2+} alkaline earth cation complexes. We therefore decided to calculate by FEP the relative stabilities of the Mg^{2+}, Ca^{2+}, Sr^{2+} and Ba^{2+} complexes of **L** in water. Experimental stability constants have been determined in methanol instead of water where **L** is nearly insoluble.[6] We chose, however, water as a solvent, because the parameters used to describe the M^{2+} cation have been fitted to reproduce the relative free energies of hydration[20] and we checked that they are nearly identical to the relative free energies of solvation in methanol. On the other hand, as will be shown in the following, the conformation of the complexes and the extent of cation shielding should be similar in both solvents.

Experimental

Synthesis

Complexation occurs in solution as shown by the upfield shift experienced by the axial protons of the Ar–CH_2–Ar bridge ($\Delta\delta$ = 1.10) and by the amide OCH_2 protons ($\Delta\delta$ = 0.14) compared with the free ligand.[7]

The amide ligand (26 mg) and strontium picrate·nH_2O (15 mg) have been suspended in $CHCl_3$ (3 cm^3) and propan-1-ol (4 cm^3) and warmed until the solid dissolves. Upon cooling, crystals are formed, which are collected and used for the X-ray and ^1H NMR spectral analyses. δ_H($CDCl_3$, 300 MHz) 8.74 (2 H, s, Pic), 7.17 (8 H, s, ArH), 4.88 (8 H, s, OCH_2CO), 4.20 (4 H, s, H_{ax}), 3.5–3.2 (20 H, m, H_{eq} and NCH_2), 1.3–0.8 (24 H, m, $NCCH_3$) and 1.13 [(36 H, s, $C(CH_3)_3$].

Table 1 Experimental data for the X-ray diffraction studies of the L·Sr(Pic)$_2$ complex

Formula	$C_{80}H_{104}N_{10}O_{22}Sr·CHCl_3$
Crystal system	Triclinic
Space group	*P*1
Cell parameters at 295 K[a]	
a/Å	13.125(6)
b/Å	14.355(6)
c/Å	13.043(6)
α/degrees	77.44(2)
β/degrees	80.70(2)
γ/degrees	72.05(2)
V/Å^3	2270(2)
Z	1
D_{calcd}/g cm^{-3}	1.291
F(000)	926
Mol. wt.	1764.75
Linear abs. coeff./cm^{-1}	22.46
Diffractometer	Siemens AED
Scan type	$\theta/2\theta$
Scan speed/degrees min^{-1}	3–12
Scan width/degrees	$(\theta - 0.65), [\theta + (0.65 + \Delta\lambda\lambda^{-1})\text{tg}\,\theta]$
Radiation	Cu-Kα (1.541 78 Å)
2θ Range/degrees	6–140
Reflections measured	$\pm h, \pm k, \pm l$
Total data measured	9005
Criterion for observed	$I \geqslant 2\sigma(I)$
Observed data measured	8790
Unique observed data	8481
Agreement between equivalent observed reflections	0.08
No. of variables	738
Max. Δ/σ on last cycle	0.07
$R = \Sigma\|\Delta F\|/\Sigma\|F_o\|$	0.061
$R_w = \Sigma w^{\frac{1}{2}}\|\Delta F\|/\Sigma w^{\frac{1}{2}}\|F_o\|$	0.061
GOF = $[\Sigma w^{\frac{1}{2}}\|\Delta F\|^2/(\text{NO–NV})]^{\frac{1}{2}}$	1.328

[a] Unit cell parameters were obtained by least-squares analysis of the setting angles of 30 carefully centred reflections found in a random search on the reciprocal space.

X-Ray crystallography

A yellow single crystal of *ca.* 0.2 × 0.3 × 0.4 mm suitable for X-ray analysis was mounted on a glass rod without protection from the air. The crystal data and the most relevant experimental parameters used in the X-ray measurements and in the crystal structure analysis are reported in Table 1. The intensities were calculated from profile analysis according to the Lehmann and Larsen method.[22] During the systematic data collection two standard reflections, collected every 100, showed no significant fluctuations. The intensities were corrected for Lorentz and polarization, but not for absorption effects.

The structure was solved by Direct Methods using SIR92.[23] The best FOM Emap showed the coordinates of all non-hydrogen atoms with the exception of those of the $CHCl_3$ solvent molecule. The structure was completed by Fourier ΔF map and then refined by blocked full-matrix least-squares methods of F using SHELX76.[24] Parameters refined were the overall scale factor, the atomic coordinates and anisotropic thermal parameters for all the non-hydrogen atoms, with the exception of the methyl carbon atoms of the *tert*-butyl group at the phenolic unit C disordered over two different orientations and the atoms of the chloroform solvent molecule, which were refined with isotropic thermal parameters. All the hydrogen atoms were placed at their calculated positions with the geometrical constraint C–H 1.0 Å and refined 'riding' on their corresponding carbon atoms.

The atomic scattering factors of the non-hydrogen atoms were taken from Cromer and Waber,[25] the values of $\Delta f'$ and $\Delta f''$ were those of Cromer.[26] The geometrical calculations were obtained by PARST.[27]

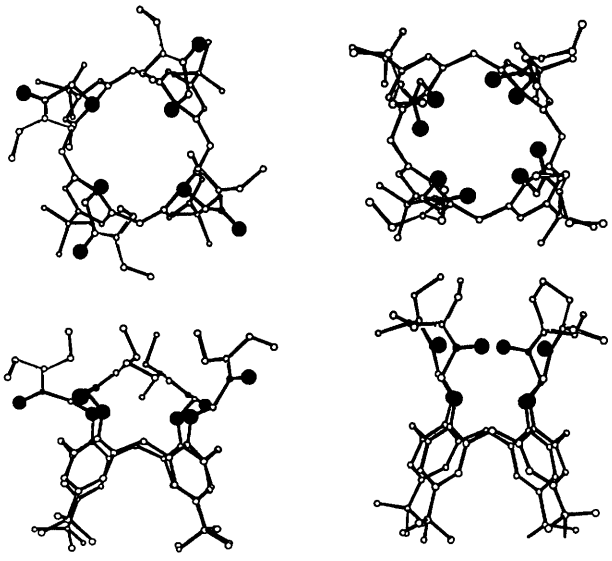

Fig. 2 The **L** host in typical diverging L_D (left) and converging L_C (right) conformations of the amidic groups (orthogonal views)

The calculations for X-ray analysis were carried out on the GOULD ENCORE91 of the Centro di Studio per la Strutturistica Diffrattometrica of C.N.R., Parma.

A list of the atomic coordinates of the non-hydrogen atoms (Table SI), thermal parameters for the non-hydrogen atoms (Table SII), the atomic coordinates of the hydrogen atoms (Table SIII) and a full list of the bond distances and angles (Table SIV) have been deposited at the Cambridge Crystallographic Data Centre.‡

Crystal data

$C_{80}H_{104}N_{10}O_{22}Sr{\cdot}CHCl_3$; $M = 1764.75$. Triclinic, $a = 13.125(6)$, $b = 14.355(6)$, $c = 13.043(6)$ Å, $\alpha = 77.44(2)$, $\beta = 80.70(2)$, $\gamma = 72.05(2)°$, space group $P\bar{1}$, $V = 2270(2)$ Å^3, $Z = 1$, $D_{calc} = 1.291$ g cm^{-3}. The most significant parameters used in the X-ray diffraction experiment are given in Table 1.

Methods of simulation

We used the AMBER software[28] for molecular mechanics, MD and FEP simulations. The potential energy, corresponding to a ball-and-stick representation of the system, is calculated *via* eqn. (1).

$$E_T = \Sigma_{bonds} K_r (r - r_{eq})^2 + \Sigma_{angles} K_\theta(\theta - \theta_{eq})^2 + \Sigma_{dihedrals}\Sigma_n V_n(1 + \cos n\varphi) + \Sigma_{i<j}[\varepsilon_{ij}(R_{ij}^*/R_{ij})^{12} - 2\varepsilon_{ij}(R_{ij}^*/R_{ij})^6 + q_i q_j/R_{ij}] \quad (1)$$

The basic underlying hypotheses, discussion of the related parameters, 'assumptions approximations and inevitable imperfections' can be found in the paper by Kollman and co-workers which describes this force field.[29] The bonds and bond angles are treated as harmonic springs, and a torsional term is associated with the dihedral angles. The interactions between atoms separated by at least three bonds are described within a pairwise additive scheme by a 1–6–12 potential. The parameters for **L**, with explicit CH_2 groups are taken from the AMBER force field[29] and from our previous work.[9,10] The atomic charges were fitted from MNDO electrostatic potentials and used without special scaling factor for 1 • • • 4 interactions. The interactions between the cations, the solvent and **L** are represented by a non-covalent model, to allow for dynamic exchange of coordination. For the alkaline earth cations, we use parameters derived from relative and absolute free energies of hydration[20] ($R^*_{Mg} = 0.787$ Å, $\varepsilon_{Mg} = 0.875$ kcal mol^{-1};§ $R^*_{Ca} = 1.326$, $\varepsilon_{Ca} = 0.449$; $R^*_{Sr} = 1.741$, $\varepsilon_{Sr} = 0.118$; $R^*_{Ba} = 2.124$, $\varepsilon_{Ba} = 0.471$). The calculations with the UO_2^{2+} cation were run with the parameters fitted from free energies of hydration: $q_u = 2.5$, $q_O = -0.25$, $R^*_U = 1.58$ Å and $\varepsilon_U = 0.12$ kcal mol^{-1}.[30] The solvent water and acetonitrile molecules are explicitly represented by three point models, using, respectively, the TIP3P and OPLS potentials fitted by Jorgensen and co-workers on the properties of the pure liquids.[21]

The procedure used to model the complexes in solution is similar to that used in related studies.[8–21] It results from a compromise between the need to represent at the molecular level an 'infinite' number of solvent molecules and the computer time limitations. The aqueous and acetonitrile solutions were

Table 2 Conditions of simulations. Size of the box, number of solvent molecules (water, acetonitrile), and time of simulation (ps)

		Box size/Å	No. solv.	*t*/ps
$L_C{\cdot}Mg^{2+}$	Gas	—	—	50
$L_C{\cdot}Ca^{2+}$	Gas	—	—	50
$L_C{\cdot}Sr^{2+}$	Gas	—	—	50
$L_C{\cdot}Ba^{2+}$	Gas	—	—	50
$L_C{\cdot}Mg^{2+}$	Water	34 × 33 × 32	973	200
$L_C{\cdot}Ca^{2+}$	Water	33 × 32 × 32	904	200
$L_C{\cdot}Sr^{2+}$	Water	34 × 33 × 32	997	500
$L_C{\cdot}Ba^{2+}$	Water	34 × 32 × 31	942	200
$L_D{\cdot}Mg^{2+}$	Water	33 × 34 × 33	1014	200
$L_D{\cdot}Ca^{2+}$	Water	33 × 34 × 33	1014	200
$L_D{\cdot}Sr^{2+}$	Water	33 × 34 × 33	1014	500
$L_D{\cdot}Ba^{2+}$	Water	33 × 34 × 33	1014	200
$L_C{\cdot}Sr^{2+}$	Acetonitrile	42 × 41 × 40	682	500
$L_D{\cdot}Mg^{2+}$	Acetonitrile	41 × 42 × 41	705	200
$L_D{\cdot}Ca^{2+}$	Acetonitrile	41 × 42 × 41	705	200
$L_D{\cdot}Sr^{2+}$	Acetonitrile	41 × 42 × 41	705	500
$L_D{\cdot}Ba^{2+}$	Acetonitrile	41 × 42 × 41	705	200
$L_C{\cdot}UO_2^{2+}$	Water	35 × 36 × 35	1399	200
$L_D{\cdot}UO_2^{2+}$	Water	35 × 36 × 35	1364	500
$L_D{\cdot}UO_2^{2+}$	Acetonitrile	41 × 42 × 41	709	200

Table 3 X-Ray structure of the **L**·Sr(Picrate)$_2$ complex: selected bond distances (Å) and angles (°) with esds in parentheses (see Fig. 3 for atom labels)

Sr–O(1A)	2.575(4)	Sr–O(2A)	2.492(6)
Sr–O(1B)	2.556(5)	Sr–O(2B)	2.489(6)
Sr–O(1C)	2.585(5)	Sr–O(2C)	2.495(5)
Sr–O(1D)	2.592(6)	Sr–O(2D)	2.530(5)
O(1A)–C(11A)	1.447(10)	C(11A)–C(12A)	1.510(10)
C(12A)–O(2A)	1.241(9)	C(12A)–N(1A)	1.331(12)
O(1B)–C(11B)	1.442(10)	C(11B)–C(12B)	1.507(11)
C(12B)–O(2B)	1.230(8)	C(12B)–N(1B)	1.340(11)
O(1C)–C(11C)	1.445(9)	C(11C)–C(12C)	1.519(15)
C(12C)–O(2C)	1.221(11)	C(12C)–N(1C)	1.323(13)
O(1D)–C(11D)	1.457(8)	C(11D)–C(12D)	1.526(11)
C(12D)–O(2D)	1.224(10)	C(12D)–N(1D)	1.324(10)
O(1A)–Sr–O(1B)	80.7(2)	O(1A)–Sr–O(1C)	128.3(2)
O(1A)–Sr–O(1D)	77.8(2)	O(1B)–Sr–O(1C)	78.4(2)
O(1B)–Sr–O(1D)	128.9(2)	O(1C)–Sr–O(1D)	79.7(2)
O(2A)–Sr–O(2B)	75.9(2)	O(2A)–Sr–O(2C)	120.7(2)
O(2A)–Sr–O(2D)	76.6(2)	O(2B)–Sr–O(2C)	120.7(2)
O(2B)–Sr–O(2D)	123.9(2)	O(2C)–Sr–O(2D)	76.5(2)
O(1A)–Sr–O(2A)	62.6(2)	O(1B)–Sr–O(2B)	62.3(2)
O(1C)–Sr–O(2C)	62.2(2)	O(1D)–Sr-O(2D)	60.9(2)

‡ For details of the CCDC deposition scheme, see 'Instructions for authors', *J. Chem. Soc., Perkin Trans. 2*, 1996, Issue 1. Any request to the CCDC for this material should quote the full literature citation and the reference number 188/4.

§ 1 cal = 4.184 J.

simulated in a 'cubic' box of 32–42 Å length, containing, respectively, about 1000 H_2O and 700 MeCN molecules, with periodic boundary conditions. Details are given in Table 2. Unless otherwise specified, a residue based cut-off of 10 Å was used for non-bonded interactions, taking the complex as a single residue.

Each system was first energy minimized by 1000 steps of conjugate gradient to avoid artificially large forces. Then the MD simulations were run at 1 atm and 300 K (N, P, T ensemble), starting with random velocities. The temperature was maintained at 300 K by velocity scaling in the gas phase, and by coupling to a thermal bath in solution. The O–H and C–H bonds in solution were constrained to constant values with the SHAKE option of AMBER,[28] in conjunction with a time step of 2 fs. In the gas phase, the time step was 1 fs, without the SHAKE option.

The differences in Gibbs free energies between M^{2+} and N^{2+} cations were calculated using the statistical perturbation FEP theory[31–34] and the windowing technique using eqns. (2) and (3).

$$\Delta G = \Sigma \Delta G_\lambda \quad (2)$$

$$\Delta G_\lambda = RT \log[\exp(E_\lambda - E_{\lambda+\Delta\lambda})/RT]_\lambda \quad (3)$$

The change in the potential energy E_λ is calculated using a linear combination of the ε and R^* parameters of the initial state ($\lambda = 1$) and final state ($\lambda = 0$): R^* and ε are calculated by eqns. (4) and (5).

$$R^*_\lambda = \lambda R^*_{M^{2+}} + (1 - \lambda) R^*_{N^{2+}} \quad (4)$$

$$\varepsilon_\lambda = \lambda \varepsilon_{M^{2+}} + (1 - \lambda) \varepsilon_{N^{2+}} \quad (5)$$

The mutation of one cation M^{2+} (free or complexed) into the next one N^{2+} was achieved in 11 windows. At each window, 1 ps of equilibration was followed by 4 ps of data collection, and the change in free energy ΔG was averaged from the forward ($\lambda + \Delta\lambda$) and backward ($\lambda - \Delta\lambda$) values.

The starting structures of the $L{\cdot}M^{2+}$ complexes were of approximate C_{4v} symmetry as in ref. 10. The 'converging' conformers L_C are derived from the X-ray structure of the K^+ complex,[7] and the 'diverging' L_D forms have been built with M^{2+} sitting on the top of the four phenolic oxygens and the four carbonyls pointing away from M^{2+} (Figs. 1 and 2). After 500 steps of energy minimization by molecular mechanics, it was shaken by MD for 50 ps in the gas phase and 200 ps in water and acetonitrile solutions. For the the L_C and L_D forms of the $L{\cdot}Sr^{2+}$ complex, the MD was run for 500 ps in water.

The energy and structural analysis of the results was performed with the MDS and DRAW software,[35] from the trajectories which were saved every 0.2 ps.

Results and discussion

Solid-state structure of the L·Sr(Picrate)$_2$·CHCl$_3$ complex

In the solid state, the complex consists of one mononuclear strontium *tert*-butyl-calix[4]arene-tetrabis(diethylamide) complex cation, two picrate anions and one $CHCl_3$ solvent molecule. Fig. 3 shows a perspective view of the complex cation together with the atomic numbering scheme adopted in each phenolic subunit. The most relevant bond distances and angles are reported in Table 3.

The Sr^{2+} ion is octacoordinated with the four phenolic oxygens and the four carbonyl oxygens of the amide chains disposed at the vertices of an almost square antiprism [O(1A)···O(1B) 3.323(7), O(1B)···O(1C) 3.248(7), O(1C)···O(1D) 3.317(7), O(1D)···O(1A) 3.246(7) Å and O(2A)···O(2B) 3.063(7), O(2B)···O(2C) 3.109(7), O(2C)···O(2D) 3.111(7), O(2D)···O(2A) 3.113(7) Å]. It is totally encapsulated in the polar niche and shielded from the interactions with the picrate anions and with the chloroform solvent molecule. Quite similar structures of the cation complexes have been observed in the L·KSCN and L·KI complexes,[7] even if in the latter ones the complexes possess four-fold symmetry. In the Sr^{2+} complex the L ligand asymmetrically chelates the metal centre and the Sr–O_{ether} distances are somewhat longer than the Sr–$O_{O=C}$ bond distances. The latter distances are quite similar to the Sr–O distances involving the β-diketonate ligands in the octacoordinate [Sr(thd)$_2$(triglyme)] complex and comparable to other Sr^{2+} complexes when the differences in the overall coordination numbers are considered.[36]

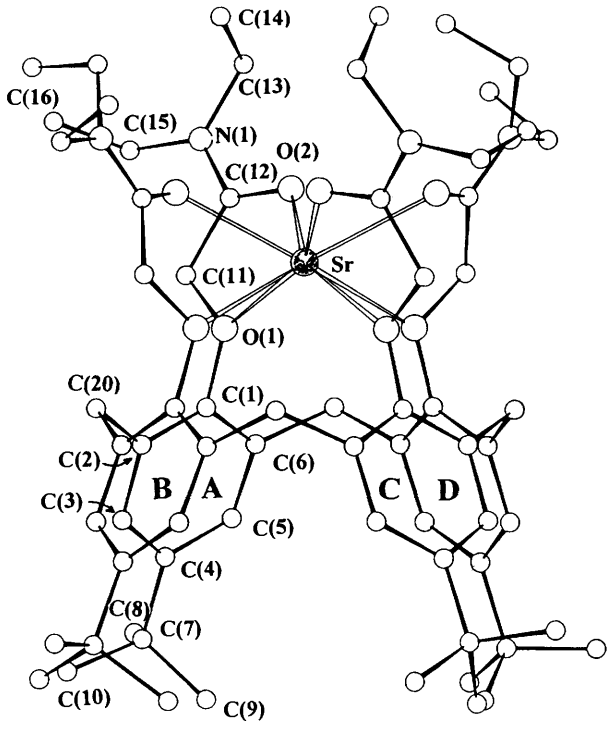

Fig. 3 X-Ray structure of the L·Sr(Picrate)$_2$ complex: perspective view. The hydrogens atoms have been omitted for clarity.

Table 4 X-Ray structures of $L{\cdot}M^{n+}$ complexes: comparison between interatomic M···O bond distances (Å)

	Bond distances d/Å	
Complex	$M^{n+}\cdots O_{ether}$	$M^{n+}\cdots O_{O=C}$
L·Sr(Pic)$_2$	2.577(5) av.	2.501(6) av.
L·KSCN	2.708(7)	2.74(1)
L·KI	2.702(11)	2.70(3)

The four O_{ether} oxygen atoms are coplanar within the esds, whereas the four carbonyl oxygens slightly deviate from the least-squares plane through them of 0.026(6) Å [O(2A) and O(2C)] and −0.026(6) Å [O(2B) and O(2D)].

The comparison of the M–O bond distances in the L·Sr(Pic)$_2$ with those observed in the L·KSCN and L·KI complexes is reported in Table 4 and shows that the Sr^{2+}–O_{ether} distances are shortened with respect of K^+–O_{ether} less than the differences (0.25 Å) in the atomic radii of Sr^{2+} (1.26 Å) and K^+ (1.51 Å),[37] suggesting that the calix[4]arene ligand does not provide optimal interactions with the two ions.

However, the structure of the ligand in the Sr^{2+} complex is only slightly different from that observed in the two K^+ complexes. Apart from a slight deviation from the four-fold symmetry and insignificant differences in the orientations of the terminal ethyl groups, in the L·Sr(Pic)$_2$ complex the dihedral

angles δ formed by the four phenolic rings and the molecular reference plane R[38] are A–R 114.4(2), B–R 112.7(2), C–R 114.9(2) and D–R 110.9(2)°, close to the value of 113.3(4)° observed in the two K^+ complexes. The values of the dihedral angles around the methylene bridges[39] reported in Table 5 give the complete and unequivocal description of the conformation of the calix[4]arene moiety. Using the sequence of signs of the conformational parameters the molecular conformation can be represented by the symbol $C_1(+-)_4$.[39]

The crystal packing (Fig. 4) shows the two picrate anions excluded from the coordination sphere of the Sr^{2+} ion and tilted to each other at 30.6(3)°. The chloroform solvent molecule lies on them and forms an intermolecular hydrogen bond with the phenoxy oxygen of one of them: [donor···acceptor distance 3.14(2) Å, donor-H···acceptor angle 147(1)°].

Structure and solvation of the L·M^{2+} alkaline earth complexes from MD simulations in the gas phase, in water and acetonitrile solutions

In this section, we describe the complexes simulated in the gas phase and in two solvents. For each cation, two simulations were performed, starting, respectively, with the converging L_C and with the diverging L_D conformations of the amidic carbonyls (Fig. 2). All L_C complexes remained of L_C type after 200 ps or more of dynamics. For a given M^{2+} cation, their structure is almost identical in the gas phase as in solution. This is why we report the results of all complexes in water only (Table 6). The gas-phase results are provided as supplementary material (Table SV).¶ Given the focus on the L·Sr^{2+} complex, representative parameters are also reported (Table 6) in the three phases.

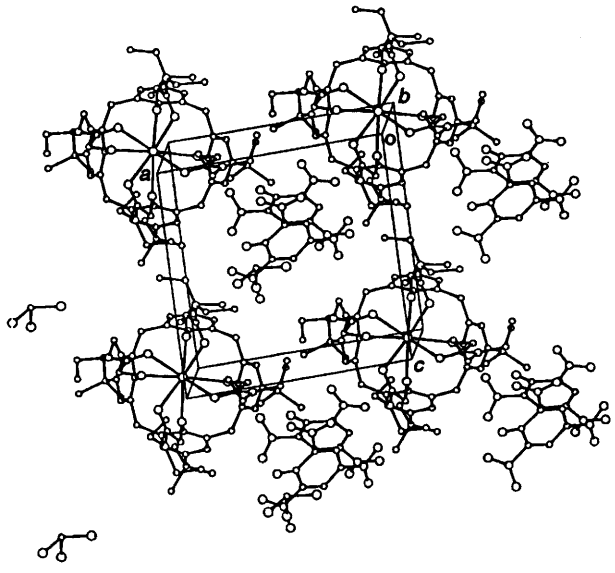

Fig. 4 Perspective view of the crystal packing of the complex L·Sr(Picrate)$_2$·$CHCl_3$

Structures simulated in the gas phase. In the gas phase, all complexes adopt rapidly a converging orientation, independently of the starting L_C or L_D conformation. The cations are coordinated to the four O_{ether} and to the four $O_{C=O}$ carbonyl oxygens (Table 6). The $M^{2+}\cdots O_{C=O}$ distances are somewhat larger than the $M^{2+}\cdots O_{ether}$ distances (Δ = 0.3 Å with Ca^{2+} and Sr^{2+}, 0.4 Å with Ba^{2+}). In the Mg^{2+} complex, the cation, too small for the ligand, is closer to the $O_{C=O}$ oxygens (Δ = 1.0 Å). As expected, when the size of M^{2+} increases, the $M^{2+}\cdots O_{C=O}$ distances increase (from 1.93 for Mg^{2+} to 2.64 Å for Ba^{2+}) as do the $M^{2+}\cdots O_{ether}$ distances (from 2.05 for Mg^{2+} to 2.60 Å for Ba^{2+}).

The carbonyl dipoles point roughly to the C_4 symmetry axis in small cation complexes. However, as M^{2+} gets bigger, they are pushed somewhat by the cation which makes more tangential instead of 'linear' contacts. The $M^{2+}\cdots O{=}C$ angles decrease from 121 (Mg^{2+}) to 115° (Ba^{2+}).

¶ Suppl. Pub. 57148 (2 pp.). For details of the British Library Supplementary Publications Scheme see 'Instructions for Authors (1996)', *J. Chem. Soc., Perkin Trans. 2*, 1996, issue 1.

Table 5 Dihedral angles C_{ar}–CH_2–C_{ar}, φ and χ (°), of the calculated L·Sr^{2+} complex in water, and of the X-ray structure of L·Sr(Picrate)$_2$

	Water[a]		X-Ray	
	φ	χ	φ	χ
A–B	82.9	−83.2	77.2(9)	−75.2(8)
B–C	82.3	−83.4	76.6(8)	−78.2(8)
C–D	82.7	−83.8	78.4(8)	−74.5(9)
D–E	82.6	−83.3	74.4(8)	−80.0(8)

[a] In the gas phase and in acetonitrile solution, the angles are within 0.5° identical to those in water.

Table 6 L·M^{2+} complexes (converging L_C forms) simulated *in vacuo*, in acetonitrile and in water: average structural parameters (after 50 ps in the gas phase and 200 ps in solution, 500 ps for L·Sr^{2+} in water and acetonitrile). Comparison with X-ray data of the L·Sr^{2+} complexes

	L_C·Sr^{2+} Gas	L_C·Mg^{2+} Water	L_C·Ca^{2+} Water	L_C·Sr^{2+} Water	L_C·Ba^{2+} Water	L_C·UO_2^{2+} Water	L_C·Sr^{2+} Acetonitrile	L_D·UO_2^{2+} Acetonitrile	L_C·Sr^{2+} X-Ray
$M^{2+}\cdots O{=}C_A$ [a,b]	2.46	1.92	2.26	2.47	2.71	2.77	2.51	3.12	2.42
$M^{2+}\cdots O{=}C_B$	2.48	4.07	2.25	2.47	2.68	2.82	2.52	3.14	2.48
$M^{2+}\cdots O{=}C_C$	2.47	3.36	2.25	2.48	2.67	2.80	2.50	3.17	2.49
$M^{2+}\cdots O{=}C_D$	2.47	3.98	2.26	2.48	2.69	2.82	2.51	3.28	2.53
$M^{2+}\cdots O_{ether}$ [c]	2.44	1.95	2.43	2.44	2.66	3.40	2.44	2.50	2.58
$C_A{=}O\cdots O{=}C_C$ [d]	4.19	2.72	3.88	4.17	5.03	5.55	4.16	5.46	4.43
$C_B{=}O\cdots O{=}C_D$	4.20	6.60	3.84	4.17	4.99	5.65	4.16	5.60	4.33
$O_{etherA}\cdots O_{etherC}$ [e]	4.39	3.79	4.18	4.36	4.46	4.80	4.39	4.85	4.64
$O_{etherB}\cdots O_{etherD}$	4.38	3.99	4.19	4.36	4.47	4.82	4.38	4.85	4.64
$C_{Bu^tA}\cdots C_{Bu^tC}$ [f]	8.92	10.26	9.05	8.89	8.80	8.57	9.04	8.58	9.23
$C_{Bu^tB}\cdots C_{Bu^tD}$	8.94	9.15	9.01	8.87	8.74	8.68	9.06	8.64	8.73
ω_{AC} [g]	47	69	51	48	46	39	49	39	49
ω_{BD}	47	54	51	47	45	40	49	40	43
$M^{2+}/O{=}C_A$ [h]	117	119	120	116	115	105	115	105	118
$M^{2+}/O{=}C_B$	115	84	121	116	111	103	115	102	117
$M^{2+}/O{=}C_C$	117	91	120	115	115	99	116	106	119
$M^{2+}/O{=}C_D$	116	81	120	114	115	98	114	97	116

[a] The A, B, C, D indices correspond to the residues defined in Fig. 1. Average distances (Å) between [b] M^{2+} and carbonyl oxygens, [c] M^{2+} and ether oxygens (average value over the four ether oxygens), [d] carbonyl oxygens, [e] ether oxygens, [f] central C atoms of *tert*-butyl. [g] Angles between opposite aromatic cycles. [h] Angles between M^{2+} and O=C.

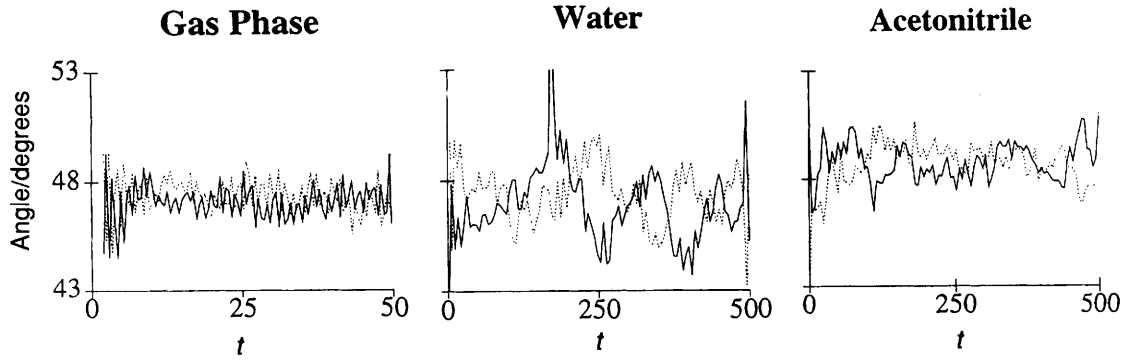

Fig. 5 Time evolution of the ω_{AC} and ω_{BD} angles between opposed aromatic rings of the $L{\cdot}Sr^{2+}$ complex in the gas phase, in water and in acetonitrile solutions (L_C form); time in ps

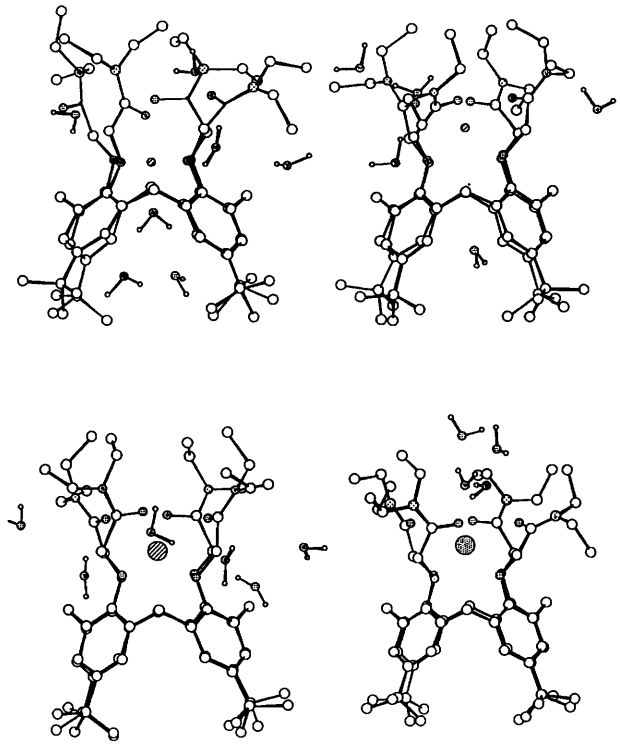

Fig. 6 Mg^{2+}, Ca^{2+} (top), Sr^{2+} and Ba^{2+} (bottom) complexes of **L** in water (converging L_C forms). Snapshots after 200 ps of MD, including selected first shell solvent molecules.

The complexed ligand **L** has on average C_4 symmetry, concerning its cone and its lower rim substituents, as seen from average parameters reported in Table 6. However, as the size of M^{2+} increases, the structure of **L** relaxes: at the lower rim, the distances between opposite $O_{C=O}$ oxygens increase on average from 3.79 (Mg^{2+}) to 4.69 Å (Ba^{2+}) and opposite O_{ether} oxygens from 3.91 (Mg^{2+}) to 4.54 Å (Ba^{2+}), while at the upper rim the distances between opposite C_{Bu^t} atoms decrease from *ca.* 9.33 (Mg^{2+}) to 8.78 Å (Ba^{2+}). There is thus some cation dependent top–bottom coupling.

The time dependence of the top–bottom coupling is illustrated by the angles ω_{AC} and ω_{BD} between planes of opposite aromatic rings (Fig. 5) for the Sr^{2+} complex: both angles display small anticorrelated oscillations of a few degrees. Thus, instantaneously, the cone is not exactly of C_{4v} symmetry, but its time average structure is C_{4v}.

Structures simulated in aqueous solution. In water, the precise conformation of the complex may be cation dependent, and depend on the starting orientation of the amidic groups. When they are initially converging (L_C form), the complexes (Fig. 6) are similar to those in the gas phase. Typical structures are shown in Fig. 6. For a given cation, the average four $M^{2+} \cdots O_{C=O}$ distances are nearly identical and the complex has C_{4v} symmetry as in the gas phase. The only exception concerns $L{\cdot}Mg^{2+}$, which opens somewhat, with one short (1.92 Å) and three large distances (*ca.* 3.3–4.0 Å). This is because Mg^{2+} sits deeply inside the cavity, at only 1.8–2.0 Å of the O_{ether} oxygens. The carbonyls not bound to Mg^{2+} reorient slightly outwards, to be better solvated by water. For the other complexes, the biggest ions Ba^{2+} and Sr^{2+} are, on the average, nearly equidistant from the O_{ether} and $O_{C=O}$ oxygens (at *ca.* 2.68 and 2.46 Å, respectively), as in the gas phase.

We now consider the starting L_D diverging forms. On the same timescale of 200 ps, depending on the size of M^{2+}, these L_D complexes become more or less converging during the dynamics. This can be followed by the time evolution of the $M^{2+} \cdots O_{C=O}$ distances (Fig. 7). In the case of the $L{\cdot}Sr^{2+}$, three $O_{C=O}$ oxygens move rapidly (in less than 10 ps) from 5.5 to 2.5 Å and one $O_{C=O}$ oxygen only remains diverging. After 500 ps of MD, complete convergence is achieved and the complex becomes nearly identical to the L_C one. Thus, comparison of the structures obtained from L_C and L_D starting forms indicates that we are close to a thermodynamic equilibrium for $L{\cdot}Sr^{2+}$, where the ligand is of L_C type. For the other cation complexes, the simulation time was limited to 200 ps and no full convergence is achieved. Interestingly, the extent of ligand wrapping depends on the size of the cation (Fig. 7). For instance, with Ba^{2+}, only one $O_{C=O}$ oxygen moves (in less than 25 ps) to the cation (at *ca.* 2.7 Å), while the three others remain at *ca.* 5 Å. With a smaller complexed cation, like Ca^{2+}, two adjacent $O_{C=O}$ oxygens end up converging to the cation (at *ca.* 2.3 Å), while the two others remain at 4.6 Å until the end of the simulation. As noticed above, the Sr^{2+} complex has three carbonyls converging at 200 ps. The $L{\cdot}Mg^{2+}$ 'diverging' complex does not follow this sequence, since Mg^{2+} sits more deeply in the pseudo-cavity than the other ions. After 200 ps, the $Mg^{2+} \cdots O_{C=O}$ distances range from 3.7 to 4.9 Å.

Structures simulated in acetonitrile solution. In acetonitrile, in contrast to the water solution, all L_D starting forms become rapidly 'converging'. The time evolution of the $M^{2+} \cdots O_{C=O}$ distances (Fig. 7) shows that convergence from L_D to L_C orientations of the amidic oxygens takes places more rapidly in acetonitrile (less than 100 ps) than in water, presumably because acetonitrile attracts less of the diverging carbonyl groups than water. The only exception concerns the $L{\cdot}Mg^{2+}$ complex which remains diverging with almost the same structure as in water (Fig. 6), *i.e.* with Mg^{2+} sitting deeply inside the cavity, between the O_{ether} oxygens. Conversely, the $L{\cdot}Sr^{2+}$ complex (Fig. 8), simulated starting with converging carbonyls (L_C form) remains so during the whole simulation. It displays similar structural parameters in water and *in vacuo* (Table 6). Its four C_{ar}–CH_2–C_{ar} (φ, χ) average angles are within 0.5° identical in the gas phase, in water and in acetonitrile: $\varphi = 82.5°$ and $\chi = -83.7°$. On the time average, the opening angles ω_{AC} and ω_{DB} of the cone are also nearly the same in acetonitrile (49°, 49°) as in

Table 7 $L{\cdot}M^{2+}$ complexes (converging L_C forms) simulated *in vacuo*, in acetonitrile and in water: average energies (kcal mol^{-1})

		Interaction energies, E/kcal mol^{-1}				
		M^{2+}–L	M^{2+}–solvent	L–solvent	E_L/kcal mol^{-1} [a]	% Amidic [b]
Gas	Mg^{2+}	−487	—	—	474	67
	Ca^{2+}	−424	—	—	455	76
	Sr^{2+}	−367	—	—	444	79
	Ba^{2+}	−316	—	—	438	83
Water	Mg^{2+}	−488	−196	−54	423	66
	Ca^{2+}	−403	−116	−58	433	76
	Sr^{2+}	−367	−114	−53	395	79
	Ba^{2+}	−308	−158	−36	387	81
	UO_2^{2+}	−224	−72	−71	409	73
Acetonitrile	Mg^{2+}	−342	−190	−56	425	44
	Ca^{2+}	−422	−118	−73	479	75
	Sr^{2+}	−364	−91	−80	420	79
	Ba^{2+}	−310	−148	−61	468	84
	UO_2^{2+}	−223	−59	−83	447	74

[a] Ligand internal energy. [b] Relative contribution of the amidic part to the cation–ligand interaction energy (see Fig. 1).

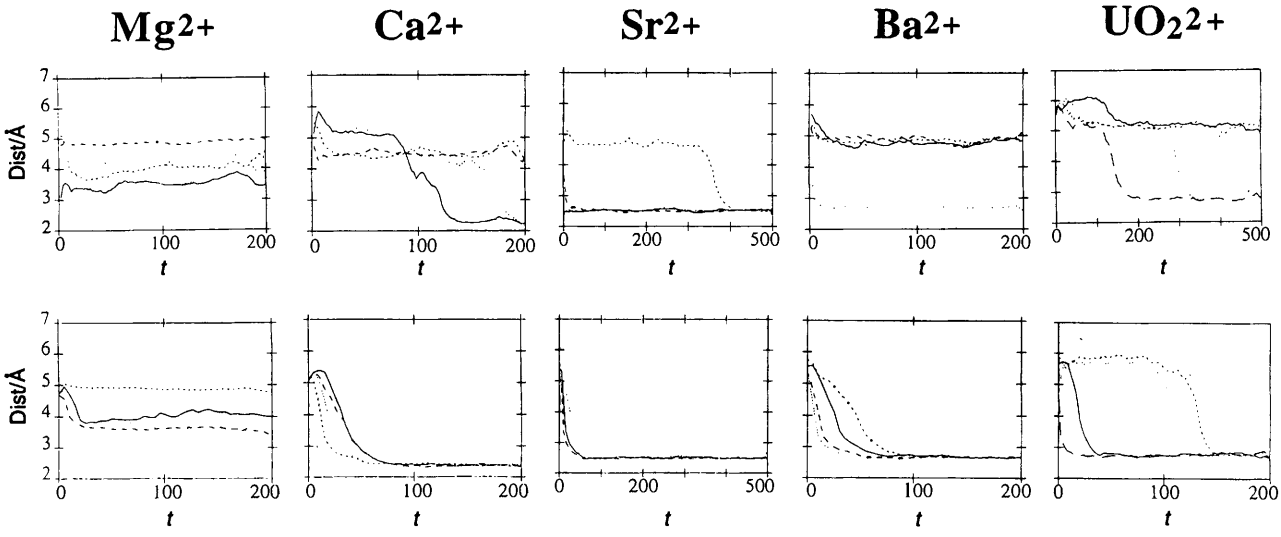

Fig. 7 Time evolution of the $M^{2+} \cdots O{=}C$ distances in water (top) and in acetonitrile (bottom) starting with the four diverging carbonyls (L_D forms); time in ps

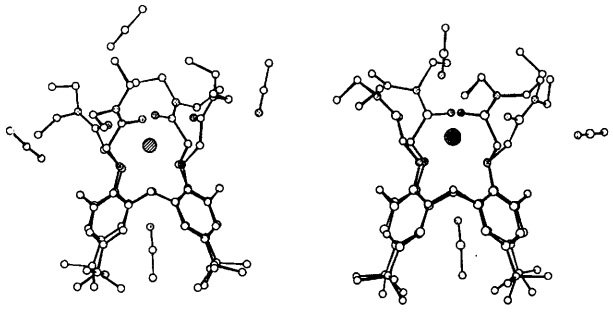

Fig. 8 $L{\cdot}Sr^{2+}$ and $L{\cdot}Ba^{2+}$ complexes in acetonitrile (converging L_C forms). Snapshots after 200 ps of MD, including selected first shell solvent molecules.

water (48°, 47°) or in the gas phase (47°, 47°), indicating a somewhat more symmetrical form than in the solid state (49°, 43°). To investigate further whether this corresponds to a time average of stable asymmetrical forms, we compared two $L{\cdot}Sr^{2+}$ complexes extracted from the dynamics in acetonitrile: one with a 'rectangular' and one with a 'squared' cone. In fact, after energy minimization, the two forms become within 0.05 Å identical with a 'squared' cone. Therefore, the slight asymmetry of the cone in the solid state is suggested not to result from intrinsic conformational effects, but from perturbations brought about by the environment in the crystal.

At a more quantitative level, some solvent dependent differences may be noticed. For instance, for the $L{\cdot}Sr^{2+}$ complex, the $Sr^{2+} \cdots O_{C=O}$ distances are *ca.* 0.04 Å longer in acetonitrile than in water or in the gas phase, presumably as a result of the difference in the content of the cone (see discussion section): it contains one MeCN molecule in acetonitrile solution, but is empty in the two other phases, as in the solid state. Another interesting difference concerns the oscillations of the ω_{AC} and ω_{BD} angles (Fig. 5), which have smaller amplitudes in acetonitrile than in water, probably also related to the above mentioned solvent content of the cone.

Energy analysis of the L_C complexes in solution. In this section, we analyse the average total potential energy in terms of interactions between L and M^{2+} ($E_{L\text{-}M^{2+}}$), of the interaction between the solvent and L ($E_{L\text{-solvent}}$) or the cation ($E_{M^{2+}\text{-solvent}}$). These values are reported in Table 7 for the L_C complexes. In water, they were obtained with L_C starting forms, but in acetonitrile, they are taken from the last sets of the simulation of L_D forms, which became of L_C type (except for the Mg^{2+} complex).

We first consider the cation ligand interaction energies, which are highly attractive and follow the same trend in water as in acetonitrile. (From Ba^{2+} to Ca^{2+}, these interactions increase by more than 100 kcal mol^{-1}.) The Mg^{2+} complex falls off the series, because it is L_C in water, but L_D-like in acetonitrile.

The contribution of the amidic groups (see Fig. 1) to $E_{L\text{-}M^{2+}}$ can be extracted from the calculations. It is clear indeed from structural features that these groups play a major role in M^{2+}

complexation. Since the unsubstituted calix[4]arene does not complex ions in methanol and acetonitrile solution, the calixarene core seems to act simply as an anchoring platform for the carbonyl binding sites. In fact, in the two solvents simulated here the relative contribution of the amidic groups is clearly dominant and increases from Ca^{2+} to Ba^{2+} from 75 to 84% in acetonitrile and 76 to 81% in water (Table 7). This is consistent with the structural features noted above: as the cation gets bigger, it is less encapsulated and more 'in contact' with the carbonyls (Fig. 6).

Another energy component of interest concerns the interaction energy $E_{M^{2+}\text{-solvent}}$ between the M^{2+} cation and the solvent. First, it is attractive in all cases (from −197 to −116 kcal mol^{-1} in water and from −91 to −190 kcal mol^{-1} in acetonitrile). This means that, although the cation is shielded by **L**, its electric field induces an attractive orientation of the water or acetonitrile dipoles. Interestingly, in water, it increases from Ca^{2+} to Ba^{2+} (−116 and −158 kcal mol^{-1}, respectively), despite the fact that the water affinity of the free cations decreases in this series. This is indicative of increased solvent coordination to the complexed cation. In particular, Ba^{2+} is in direct contact with one H_2O molecule since the 'carbonyl gate' of **L**·Ba^{2+}, pushed by this large cation, opens somewhat. In acetonitrile, a similar non-regular evolution from Ca^{2+} to Ba^{2+} is also observed due to differences in cation shielding from the solvent and the position inside the host. As in water, Ba^{2+} interacts more than Sr^{2+} or Ca^{2+} with the solvent. In many configurations, one MeCN molecule is coordinated to Ba^{2+} (Fig. 8) but not to the other cations.

These energy features of the L_C complexes are consistent with the analysis of radial distribution functions of O_{water} or N_{MeCN}, which display no peak below 5 Å around the Mg^{2+}, Ca^{2+} and Sr^{2+} complexed cations. The **L**·Ba^{2+} complex displays a peak at 2.8 Å, integrating to 0.9 water molecules. Concerning the L_D forms they display, at the beginning of the simulation, less shielding than L_C forms, and all cations are coordinated to solvent molecules, with a clear peak at 2–2.6 Å. However, as they evolve to more converging forms, solvent is stripped from M^{2+}. In particular, after 500 ps, Sr^{2+} is completely shielded from water or acetonitrile.

Finally, note that the ligand–solvent interaction energies are all attractive (from −36 to −54 kcal mol^{-1} in water and −56 to −80 kcal mol^{-1} in acetonitrile; see Table 7). Interestingly, in the Ba^{2+} complex, the ligand **L** is least well solvated in both solvents. This is because the water or acetonitrile molecule coordinated to Ba^{2+} has repulsive interactions with **L**.

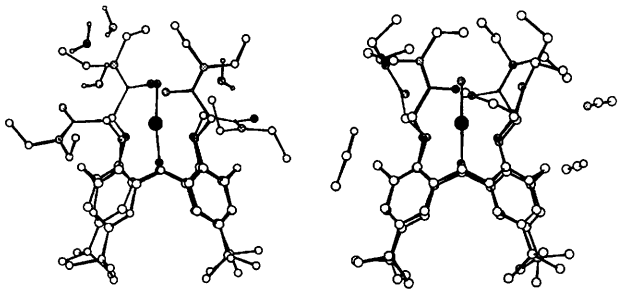

Fig. 9 **L**·UO_2^{2+} complex in water (left) and in acetonitrile (right): L_D conformer after 200 ps

The **L**·UO_2^{2+} complex simulated in water and acetonitrile

The **L**·UO_2^{2+} complex has been simulated in water and in acetonitrile, starting also with converging L_C and diverging L_d conformations of **L** with UO_2^{2+} sitting on the four-fold symmetry axis. In both solvents, after 200 ps, the L_C complex remains 'closed', with the cation encapsulated in the polar niche. In acetonitrile, the L_D starting form converges to a structure identical to the L_C one, where the cation sits deeply in the cavity (Fig. 9). The U atom is closer to the O_{ether} (2.5 Å) than to the $O_{C=O}$ oxygens (3.2 Å). In the three simulations, the UO_2^{2+} cation remains at the same position inside the cavity. In water, no full convergence of the carbonyls is achieved, even when the simulation was pushed up to 0.5 ns. Typically, two groups converge to the cation, while the two others remain pointing to the solvent (Fig. 9).

An important difference between spherical M^{2+} and linear UO_2^{2+} complexed cations concerns the secondary repulsive interactions between the O_{uranyl} and O_{ligand} oxygen atoms, which compete with the attraction between the U atom and **L**. Thus, although the U atom bears a charge of 2.5, *i.e.* larger than Sr^{2+}, the UO_2^{2+} cation displays much weaker attractions with **L**. In water as in acetonitrile, this difference in M^{2+}–**L** attractions amounts to *ca.* 140 kcal mol^{-1} (Table 7). Thus, the affinity of **L** for UO_2^{2+} should be much lower than for the alkaline earth cations.

Is it possible to predict the alkaline earth cation binding selectivity? FEP studies on the M^{2+} complexation by L in water

The binding selectivity of M^{2+}, relative to N^{2+} complexed by the ligand **L**, is obtained experimentally as $\Delta\Delta G_c = \Delta G_1 - \Delta G_2$. The computational procedure follows the 'alchemical route'[31] *i.e.* calculates ΔG_3 and ΔG_4 in solution. According to the thermodynamic cycle $\Delta\Delta G_c = \Delta G_3 - \Delta G_4$.

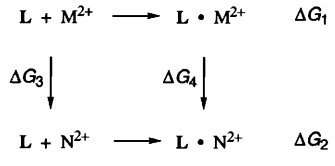

For the uncomplexed cations, our ΔG_3 values calculated in aqueous solution are nearly identical to the ΔG_3 values calculated by Åqvist, using a somewhat different water potential (SPC instead of TIP3P) and a different representation of the solvent (spherical cap, instead of cubic box with periodic boundary conditions).[20] Table 8 also shows that the calculated ΔG_3 free energies are within 0.5 kcal mol^{-1} identical in water and in methanol solutions. This is why, for the **L**·M^{2+}

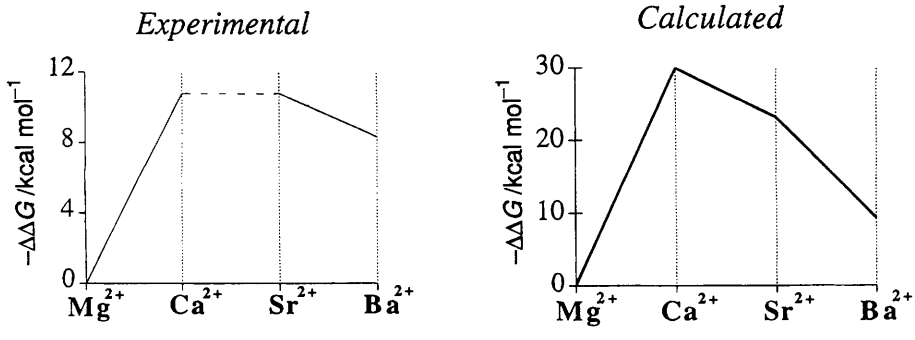

Fig. 10 Experimental and calculated relative Gibbs energies of binding of M^{2+} by **L**

Table 8 Free and complexed M^{2+} cations: calculated relative Gibbs energies ΔG_3 in water and methanol and ΔG_4 in water (kcal mol^{-1}). Relative free energies of complexation $\Delta\Delta G_c = \Delta G_3 - \Delta G_4$ in water

	ΔG_3 Water	ΔG_3 Methanol	ΔG_4 Water	$\Delta\Delta G_c$ Water
$Mg^{2+} \rightarrow Ca^{2+}$	76.6	74.9	46.7	29.9
$Ca^{2+} \rightarrow Sr^{2+}$	35.9	34.9	42.0	−6.7
$Sr^{2+} \rightarrow Ba^{2+}$	32.1	31.0	42.2	−13.8

complexes, where the cation is more or less shielded from solvent, we run the simulations in water only, since $\Delta G_{4,water}$ and $\Delta G_{4,methanol}$ should be very close.

The ΔG_4 relative free energies were obtained with the L_c starting structures, which remain converging throughout the mutation. It is clear from Table 8 that both ΔG_3 and ΔG_4 Gibbs energies increase with the size of M^{2+}. However, the $\Delta\Delta G_c = \Delta G_3 - \Delta G_4$ energy difference is positive for Mg^{2+}–Ca^{2+} and negative for Ca^{2+}–Sr^{2+} and Sr^{2+}–Ba^{2+}, as represented in Fig. 10. We therefore calculate a peak of binding selectivity for Ca^{2+}, while Mg^{2+} displays the weakest binding to **L**, in the order $Ca^{2+} > Sr^{2+} > Ba^{2+} > Mg^{2+}$. Complexation experiments in methanol solution find no complexation with Mg^{2+} and weaker complexation with Ba^{2+} (log K_s = 7.2) than with Ca^{2+} or Sr^{2+} (log K_s > 9.0). For Ca^{2+} and Sr^{2+}, no precise values could be given, because of the too high stability of the complexes. However, the Ca^{2+} complex is more stable than the Sr^{2+} complex.[6] Our calculated binding sequence is in full agreement with this sequence. For the Mg^{2+}–Ba^{2+} binding, the calculated $\Delta\Delta G_c$ (9.3 kcal mol^{-1}) is close to the experimental value (8.2 kcal mol^{-1}).

In order to investigate the role of the conformational state of the complex on the calculated ΔG_4 values, we decided to perform additional investigations on the Mg^{2+}–Ca^{2+} complexes starting with the L_D instead of the L_C conformer. As the simulated time for these mutations (50 ps) is too short to observe conformational transitions to converging L_C forms (Fig. 7), these complexes remained of L_D type. This leads for the $L{\cdot}Mg^{2+} \rightarrow L{\cdot}Ca^{2+}$ mutation to a larger ΔG_4(56.5 kcal mol^{-1}) and smaller $\Delta\Delta G_c$(20.1 kcal mol^{-1}) than when the L_C form was used (ΔG_4 = 46.7 kcal mol^{-1}; $\Delta\Delta G_c$ = 29.9 kcal mol^{-1}). A clear preference for Ca^{2+} over Mg^{2+} complexation is still found, but is somewhat lower than with the L_C form.

Thus, to conclude this section, the free energy perturbation simulations using pairwise additive potentials correctly reproduce trends in relative binding selectivies of alkaline earth M^{2+} cations.

Discussion and conclusions

The design of ligands for selective complexation of ions using the concept of host–guest complementarity requires a precise knowledge of structures in solution. Spectroscopic methods such as NMR, although very useful to prove the formation of complexes, provide time average pictures which may not correspond to energy minima and are generally not precise enough to determine precisely the conformation of the ligand and to which extent it wraps around the cation. Indirect evidence of the conformational rearrangements which occur upon complexation may be obtained from thermodynamic data.[40] The translation of such data into precise structural features remains quite speculative. Structures determined in the solid state, when good crystals are available, are more informative about precise structural parameters, but they may not be representative of structures in solution. It is not clear also to which extent the structure of a given cation complex is retained upon substitution of this cation by a slightly different one. Computer simulations taking into account explicitly the dynamic features of the solvent and the solute provide microscopic views of the time evolution of structures in solution. They provide a powerful basis for understanding the interplay between intrinsic conformational preferences and solvation effects. Systems can be selected at will, immersed in solution and simulated. In macrocyclic chemistry, the 18-crown-6 molecule has been the most extensively studied one and has become to computer modelling what the hydrogen molecule has been to quantum chemists. The many computer simulations on macrocyclic ionophores such as crown ethers, cryptands, calixarenes, which are documented as much as possible from the experimental side, displayed two complementary facets: (*i*) evaluation and test of the simulation methods and (*ii*) gain of deeper insights into these systems. Examples can be found in refs. 8–19 and in review papers of Toner,[41] Kollman and Merz[42] and Wipff.[43]

In this paper, we have reported an MD study on the alkaline earth cation complexes of the conformationally mobile *tert* butyl-calix[4]arene-tetradiethylamide ligand **L** and an X-ray structure of the $L{\cdot}Sr(Picrate)_2$ complex. Both studies performed independently indicate that, although the cation binding sites of the free ligand are mobile and not preorganized for cation complexation,[7] they display, within the complexes, a pseudo-cavity where the M^{2+} cation is encapsulated. The fact that, in the solid state, the cation has no coordination to its counterions indicates that the ligand **L** provides an adequate surrounding to the cation, as likely do other related carbonyl-containing calixarene derivatives.[44] From the computational side, this validates the neglect of counterions in the simulations. Whether such ion pair separation would be observed with trivalent cations such as lanthanide complexes[45] remains to be investigated.

Solvent dependent ligand wrapping around the complexed cation. Comparison of M^{2+} and M^+ cations

The computations reported here show that the ligand wraps around the complexed M^{2+} cation, more than it does around M^+ alkali cations.[9,10] In acetonitrile and in water, converging forms should display the largest population. The difference between water and acetonitrile solutions of $L{\cdot}M^{2+}$ concerns the rate of conformational change of **L** from L_D to L_C forms. In contrast to the $L{\cdot}M^+$ complexes, no L_C to L_D conversion is observed for $L{\cdot}M^{2+}$ complexes. In particular, the solid-state structure of the $L{\cdot}Sr^{2+}$ is close to the structure simulated in aqueous and non-aqueous solutions, whereas the solid-state structure of the $L{\cdot}K^+$ complex does not represent its structures in water, nor the structures of other alkali cation $L{\cdot}M^+$ complexes. The simulated $L{\cdot}M^+$ complexes display dynamic exchanges between converging and diverging forms, while the $L{\cdot}M^{2+}$ do not. In particular, no loss of $M^{2+} \cdots$ carbonyl coordination is observed during our MD simulations, in contrast to the $L{\cdot}M^+$ complexes where the cation–ligand attractions are smaller than in $L{\cdot}M^{2+}$. According to thermodynamic data on M^{2+} complexation in methanol, the entropic $T\Delta S$ term is favourable and larger than the ΔH enthalpic component.[6] This is consistent with our finding that the structures are more 'closed', and the M^{2+} cations are more shielded than the alkali cations M^+. Thus, complexation releases more solvent from M^{2+}, which increases the entropy of the system.

About the shape of the cone

The shape of the cone can be monitored by the ω_{AC} and ω_{BD} angles between opposed aromatic rings, by the $d_{O(A)-O(C)}$ and $d_{O(B)-O(D)}$ distances between ether oxygens at the lower rim and by the $d_{C(A)-C(C)}$ and $d_{C(B)-C(D)}$ distances between the central C atoms of *tert*-butyl groups at the upper rim (Table 6). Average values (Table 6) indicate that the cone is nearly square in all

complexes. The time evolution of these parameters (Fig. 5) shows, however, that the cone oscillates between 'rectangular' forms, with anticorrelated motions of A–C or B–D opposed moieties. The M^{2+} cations complexed in the pseudo-cavity modulate somewhat the cone shape due to the top–bottom coupling. For instance, in water, as M^{2+} gets bigger, from Ca^{2+} to Ba^{2+}, the $d_{OA\cdots OC}$ and $d_{OB\cdots OD}$ distances between ether oxygens increase by *ca.* 0.28 Å, while the $d_{C(A)\cdots C(C)}$ and $d_{C(B)\cdots C(D)}$ distances between central Bu^t carbons decreases by *ca.* 0.25 Å (Table 6).

The question of solvent inside the cone

In some of the complexes, solvent molecules diffuse inside the cone during the dynamics. In water, the cone of **L**·Mg^{2+} and **L**·Ca^{2+} complexes contains, respectively, two and one water molecules, oriented with the oxygen atom pointing to the cation (Fig. 6). The cone of **L**·Sr^{2+} and **L**·Ba^{2+} complexes contains no water. This evolution of solvent content of the cone may be related to the cation induced top–bottom coupling (see above). For the Mg^{2+} complex, the cone is most open and asymmetrical (ω_{AC} = 69°, ω_{BD} = 54°) and contains three water molecules (Fig. 6). The cone of the Ca^{2+} complex, more 'square' and closed ($\omega_{AC} = \omega_{BD}$ = 51°) contains one water molecule only. In the Ba^{2+} complex the cone is most 'closed' and symmetrical ($\omega_{AC} = \omega_{BD}$ = 46°) and empty. For the **L**·Sr^{2+} complex, simulated for a longer time (0.5 ns) than the other complexes, no water migration to the cone took place either.

In acetonitrile solution, the cone of all **L**·M^{2+} complexes contains one MeCN solvent molecule which diffused inside during the dynamics, pointing its N-terminus to the cation (Fig. 8).

This orientation of solvent molecules in the cone differs in **L**·M^{2+}, compared with **L**·M^{+} complexes or to the free ligand. In the latter, water or acetonitrile molecules were oriented with their positively charged groups pointing toward M^{+} as governed by the dipole–dipole interactions with **L**. In **L**·M^{2+} complexes, the electric field induced by the cation drives the solvent molecules with their negatively charged atoms pointing toward M^{2+}. Therefore, the acetonitrile or water orientation inside the cone of **L**·M^{2+} is driven by dipole–charge interactions with the complexed M^{2+} cation, rather than by the dipole–dipole interactions with the phenolic residues of the cone.

Because their shape and size are more complementary to the cone, acetonitrile molecules diffuse more easily than water inside the cone, since all **L**·M^{2+} complexes contain one MeCN molecule while only **L**·Mg^{2+} and **L**·Ca^{2+} complexes contain water.

Prediction of alkaline earth relative binding affinities

Another important issue concerned the theoretical prediction of relative binding affinities of alkaline earth cations. Most of the studies reported so far dealt indeed with alkali cations. With divalent cations, it was not clear whether an empirical energy representation of non-bonded interactions by a pairwise additive potential, not including explicitly polarization and non-additive effects, could give satisfactory results. In agreement with experiment, we calculate that in aqueous solution Mg^{2+} displays the weakest binding to **L**, while Sr^{2+} and Ca^{2+} complexes are the most stable. Intrinsically (*i.e.* in the gas phase) Mg^{2+} displays the largest affinity for **L**, but taking into account the desolvation energy of the cation leads to a peak of selectivity for Sr^{2+} and Ca^{2+}. Similar FEP studies on 222·M^{2+} cryptate complexes, including counterions, also give good agreement between calculated and experimental sequences of binding in solution.[46] Such studies should therefore bring an impetus to the computer based design of ionophores selective for alkaline earth ions such as Sr^{2+} of particular interest in the context of nuclear waste separation.[47]

Acknowledgements

The authors are grateful to the CNRS for generous allocation of computer time on IDRIS and to the EEC (HCM Program ERB-CHRX-CT94-0484 and F12W-CT90-0062 contract) for support. W. G. thanks A. Varnek and E. Engler for their assistance and I. Thondorf for critical reading of the manuscript.

References

1 R. Ungaro, A. Arduini, A. Casnati, O. Ori, A. Pochini and F. Ugozzoli, in *Computational Approaches in Supramolecular Chemistry*, ed. G. Wipff, Kluwer, Dordrecht, 1994,
2 A. F. D. de-Namor, N. A. de-Sueros, M. A. McKervey, G. Barrett, F. Arnaud-Neu and M. J. Schwing-Weill, *J. Chem. Soc., Chem. Commun.*, 1991, 1546.
3 V. Böhmer, *Angew. Chem., Int. Ed. Engl.*, 1995, **34**, 713 and refs. cited therein.
4 F. Arnaud-Neu, M. J. Schwing-Weil, K. Ziat, S. Cremin, S. J. Harris and M. A. M. Kervey, *New J. Chem.*, 1991, **15**, 33.
5 F. Arnaud-Neu, S. Fanni, L. Guerra, W. McGregor, K. Ziat, J.-M. Schwing-Weill, G. Barret, M. A. McKervey, D. Marrs and E. M. Seward, *J. Chem. Soc., Perkin Trans. 2*, 1995, 113.
6 F. Arnaud-Neu, G. Barrett, S. Fanni, D. Marrs, W. McGregor, M. A. McKervey, M.-J. Schwing-Weill, V. Vetrogon and S. J. Wechsler, *Chem. Soc., Perkin Trans. 2*, 1995, 453.
7 A. Arduini, E. Ghidini, A. Pochini, R. Ungaro, G. D. Andreetti, G. Calestani and F. Ugozzoli, *J. Incl. Phenom.*, 1988, **6**, 119.
8 G. Wipff and L. Toxler, in *Computational Approaches in Supramolecular Chemistry*, ed. G. Wipff, Kluwer, Dordrecht, 1994, 319.
9 A. Varnek and G. Wipff, *J. Phys. Chem.*, 1993, **97**, 10 840.
10 P. Guilbaud, A. Varnek and G. Wipff, *J. Am. Chem. Soc.*, 1993, **115**, 8298.
11 M. H. Mazor, J. A. McCammon and T. P. Lybrand, *J. Am. Chem. Soc.*, 1990, **112**, 4411.
12 P. Auffinger and G. Wipff, *J. Chim. Phys.*, 1991, **88**, 2525.
13 L. Troxler and G. Wipff, *J. Am. Chem. Soc.*, 1994, **116**, 1468.
14 S. Miyamoto and P. A. Kollman, *J. Am. Chem. Soc.*, 1992, **114**, 3668.
15 P. D. J. Grootenhuis, P. A. Kollman, L. C. Groenen, D. N. Reinhoudt, G. J. van Hummel, F. Ugozzoli and G. D. Andreetti, *J. Am. Chem. Soc.*, 1990, **112**, 4165.
16 M. Lauterbach and G. Wipff, *Supramol. Chem.*, 1995, **6**, 187.
17 G. Eisenman, O. Alvarez and J. Aquist, *J. Incl. Phenom. Mol. Recogn.*, 1992, **12**, 23.
18 T. J. Marrone and K. M. Merz, *J. Am. Chem. Soc.*, 1995, **117**, 779.
19 T. J. Marrone and K. M. Merz, *J. Am. Chem. Soc.*, 1992, **114**, 7542.
20 J. Åqvist, *J. Phys. Chem.*, 1990, **94**, 8021; 1994, **98**, 8253.
21 W. L. Jorgensen, J. Chandrasekhar and J. D. Madura, *J. Chem. Phys.*, 1983, **79**, 926; W. L. Jorgensen and J. M. Briggs, *Mol. Phys.*, 1988, **63**, 547.
22 M. S. Lehmann and F. K. Larsen, *Acta Crystallogr., Sect. A*, 1974, 580.
23 A. Altomare, M. C. Burla, M. Camalli, G. Cascarano, C. Giacovazzo, A. Guagliardi and G. Polidori, SIR92, *J. App. Crystallogr.* 1994, **27**, 435.
24 G. Sheldrick, SHELX76, Program for Crystal Structure Determinations, University of Cambridge, England, 1976.
25 D. T. Cromer and J. J. Waber, *International Tables for X-Ray Crystallography*, The Kynoch Press, Birmingham, England, 1974, vol. 4, Table 2.2.B.
26 D. T. Cromer, *International Tables for X-Ray Crystallography*, The Kynoch Press, Birmingham, England, 1974, vol. 4, Table 2.3.1.
27 M. Nardelli, M. PARST, *Comput. & Chem.*, 1983, **7**, 95.
28 D. A. Pearlman, D. A. Case, J. C. Cadwell, G. L. Seibel, U. C. Singh, P. Weiner and P. A. Kollman, AMBER4, University of California, San Francisco, 1991.
29 W. D. Cornell, P. Cieplak, C. I. Bayly, I. R. Gould, K. M. Merz, D. M. Ferguson, D. C. Spellmeyer, T. Fox, J. W. Caldwell and P. A. Kollman, *J. Am. Chem. Soc.*, 1995, **117**, 5197.
30 P. Guilbaud and G. Wipff, THEOCHEM, 1996, in the press.
31 T. P. Straatsma and J. A. McCammon, *Ann. Rev. Phys. Chem.*, 1992, **43**, 407; D. L. Beveridge and F. M. DiCapua, *Ann. Rev. Biophys. Biophys. Chem.*, 1989, **18**, 431.
32 U. C. Singh, F. K. Brown, P. A. Bash and P. A. Kollman, *J. Am. Chem. Soc.*, 1987, **109**, 1607.
33 P. A. Bash, U. C. Singh, R. Langridge and P. A. Kollman, *Science*, 1987, **236**, 564.
34 W. L. Jorgensen, *Acc. Chem. Res.*, 1989, **22**, 184.

35 E. Engler and G. Wipff, DRAW. A program for graphical representation and analysis of molecular trajectories in solution, Université Louis Pasteur, Strasbourg, 1994.
36 S. R. Drake, M. B. Hursthouse, K. M. Malid and A. A. S. Miller, *J. Chem. Soc., Chem. Commun.*, 1993, 478.
37 *Handbook of Chemistry and Physics*, 76th edn., ed. D. R. Lide, CRC Press, Boca Raton, FL, 1995–1996, ch. 12, pp. 14, 15.
38 M. Perrin and D. Oehler, in *Calixarenes: a Versatile Class of Macrocyclic Compounds*, eds. J. Vicens and V. Böhmer, Kluwer, Dordrecht, 1991, 65.
39 F. Ugozzoli and G. D. Andreetti, *J. Incl. Phenom. Mol. Recogn.*, 1992, **13**, 337.
40 A. F. Danil de Namor, E. Gil, M. A. Llosa Tanco, D. A. Pacheco Tanaka, L. E. Pulcha Salazar, R. A. Schulz and J. Wang, *J. Phys. Chem.*, 1995, **99**, 16 776; 16 781.
41 J.-L. Toner, in *Crown Ethers and Analogs*, ed. S. Patai, 1989, p. 77.
42 P. A. Kollman and J. K. M. Merz, *Acc. Chem. Res.*, 1990, **23**, 246.
43 G. Wipff, *J. Coord. Chem.*, 1992, **27**, 7. See also *Computational Approaches in Supramolecular Chemistry*, ed. G. Wipff, Kluwer, Dordrecht, 1994.
44 M. A. M. McKervey, personal communication. G. W. thanks Prof. McKervey for providing information on X-Ray structures of cation complexes of carbonyl containing calixarenes.
45 N. Sabbatini, M. Guardigli, A. Mecati, V. Balzani, R. Ungaro, E. Ghidini, A. Castani and A. Pocchini, *J. Chem. Soc., Chem. Commun.*, 1990, 878.
46 N. Muzet and G. Wipff, unpublished work.
47 L. Cecille, M. Casarci and L. Pietrelli, *New Separation Chemistry Techniques for Radioactive Waste and other Specific Applications*, Commission of the European Communities, Elsevier Applied Science, London and New York, 1991.

Paper 5/07832F
Received 1*st December* 1995
Accepted 1*st February* 1996